# Basic Study on Energy Storage Flywheel System With a Suspended Flywheel Rotor


Wataru TAKAHASHI
Kyushu Institute of Technology
Kitakyushu, Fukuoka 804-8550, Japan

Mochimitsu KOMORI*
Kyushu Institute of Technology
Kitakyushu, Fukuoka 804-8550, Japan

Teruo MATSUSHITA
Kyushu Institute of Technology
Kitakyushu, Fukuoka 804-8550, Japan

Naoki KOSHIZUKA
Kyushu Institute of Technology
Kitakyushu, Fukuoka 804-8550, Japan

Nobuo SAKAI
Kyushu Institute of Technology
Kitakyushu, Fukuoka 804-8550, Japan

Ken-ichi ASAMI
Kyushu Institute of Technology
Kitakyushu, Fukuoka 804-8550, Japan



**Abstract**

In this paper, a new model of energy storage flywheel system is proposed. The energy storage flywheel system is composed of a superconducting stator, a flywheel rotor, an induction motor and some positioning actuators. The flywheel rotor is suspended by a superconducting stator with one end fixed to a stable base. The paper discusses basic and dynamic characteristics of the energy storage flywheel system. As a result, displacements of the stator and the flywheel rotor are related with each other.


# 1 Introduction

Energy storage flywheel system is a very promising energy-saving technology. This is because the system is very simple and characterized by high energy density compared with other energy storage systems. High temperature superconductors with strong pinning forces are useful for such applications [1]-[4]. Moreover, there are some reports about flywheel systems using superconducting magnetic bearings (SMBs) and active magnetic bearings (AMBs) to suppress rotor vibrations [5]. Then, a new energy storage flywheel system is proposed whose concept is different from these systems. The flywheel rotor is suspended by a superconducting stator.

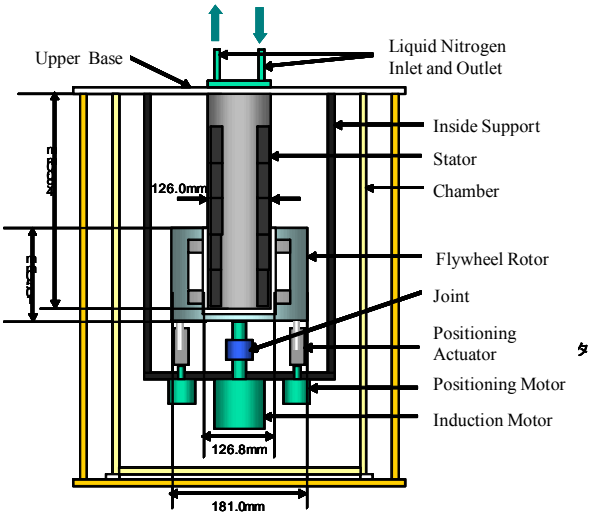


Figure 1 Schematic illustration of total energy storage flywheel system


*komori_mk@yahoo.co.jp, Department of Applied Science for Integrated System Engineering, Kyushu Institute of Technology, 1-1 Sensui, Tobata, Kitakyushu, Fukuoka 804-8550, Japan, Phone/Fax +81-93-884-3563

# 2 Energy storage flywheel system

The total system is shown in Figure 1. The flywheel energy storage system is composed of a superconducting stator, a flywheel rotor, an induction motor and some positioning actuators. The flywheel rotor is suspended by a stator whose one end is fixed to a stable base. These are set in a vacuum chamber. Liquid nitrogen flows into the superconducting stator from the top. The superconducting stator measures 126.8 mm in diameter, 460 mm in length. Figure 2(a) shows a photo of the superconducting stator which is detached from the system. The stator has doughnut-shaped superconductors (OD123.2 mm ×ID93.2 mm ×T60 mm) in the stator as shown in Figure 2(b).

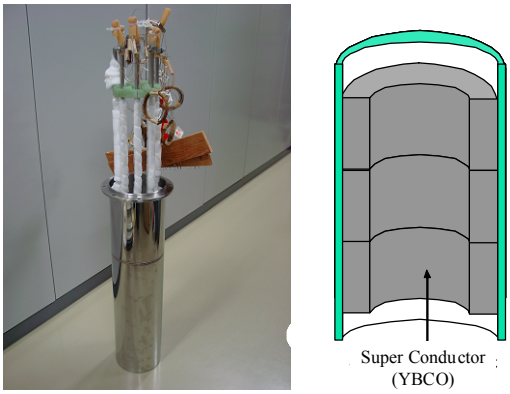


(a) (b)

Figure 2 Photo of (a) the superconducting stator and (b) the superconductors

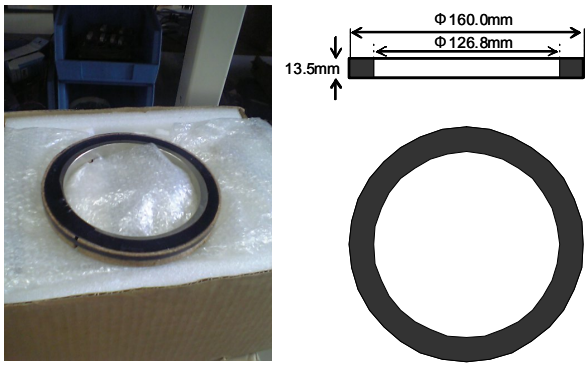


(a) (b)

Figure 3 Permanent magnet for the flywheel rotor

Figure 3 shows an NdFeB permanent magnet (OD160 mm ×ID126.8 mm ×T13.5 mm) for the flywheel rotor. As shown in Figure 1, two permanent magnets are installed in the flywheel rotor (8.9 kg, OD181 mm ×ID126.8 mm ×T105 mm). The flywheel rotor is set at one end of the stator as shown in Figure 4, where the flywheel rotor is supported by some mechanical actuators under the rotor.

# 3 Experiments and discussions (I)

## 3.1 Free-run tests

Figure 5 shows an experimental setup for free-run tests. The rotor is supported by four positioning actuators. The gap between the rotor and the stator is ≈0.8 mm. After field-cooling of superconductors in the stator, the positioning actuators separate from the flywheel rotor. The rotor is driven by the induction motor. Just after the rotation speed increases up to 1,000 rpm, the driving force of the induction motor stops. Then, the rotation speed and displacements of the rotor are measured. The displacements of upper flywheel rotor and lower flywheel rotor are

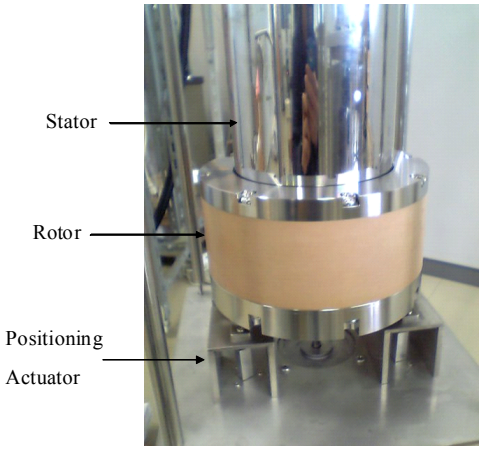


Figure 4 Flywheel rotor set at one end of the stator

measured by using two laser displacement sensors.

Figure 6 shows the experimental results of free-run tests, showing (a) natural rotational decay characteristic, (b) displacement of upper rotor and (c) displacement of lower rotor. The rotation speed decays from ≈1,000 rpm to zero for ≈1,500 s. During the rotation, the displacement pattern of upper rotor is almost the same as that of lower rotor. There are resonance rotation speeds at ≈200 s and ≈900 s, which are corresponding to ≈800 rpm and ≈300 rpm, respectively. Except for these resonance rotation speeds, the displacement is less than 0.2 mm over a wide time range.

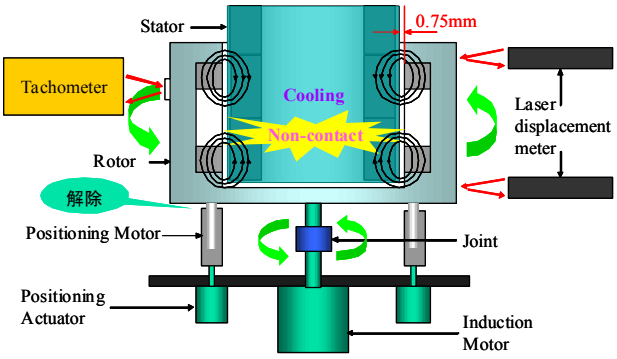


Figure 5 Experimental setup for free-run tests

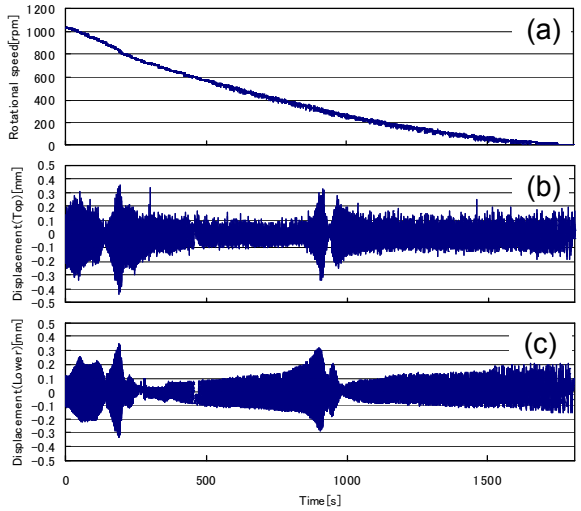


Figure 6 Experimental results of free-run tests, showing (a) natural rotation decay characteristic, (b) displacement of upper flywheel rotor and (c) displacement of lower flywheel rotor

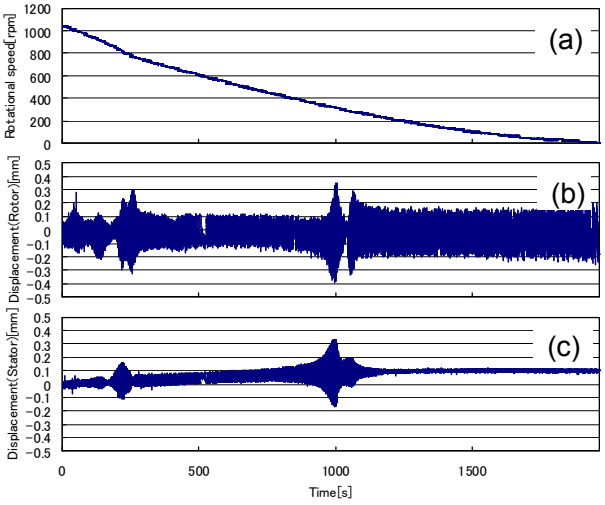


Figure 7 Experimental results of free-run tests, showing (a) natural rotation decay characteristic, (b) displacement of upper flywheel rotor and (c) stator center

Another experimental data is shown in Figure 7, representing (a) natural rotational decay characteristic, (b) displacement of upper flywheel rotor and (c) displacement of stator center. The experiment is the same as that in Figure 6. Then, the results in Figures 7(a) and (b) are almost the same as those in Figures 6(a) and (b), respectively. The displacement of stator center is generally less than 0.1 mm over a wide time range as shown in Figure 7(c). Moreover, there are some displacement peaks at $\approx$250 s and $\approx$950 s. These peaks are corresponding to the rotor peaks shown in Figure 7(b). The detail discussions are necessary in order to clarify that the displacement peaks of rotor in Figures 7(b) and (c) depend on SMB stiffness or stator stiffness.

# 4 Experiments and discussions (II)

## 4.1 Free-run tests

Figure 8 shows the experimental setup of flywheel energy storage system for impulse responses. The setup for the flywheel rotor is the same as that of rotation tests shown in Figure 1. The stator in Figure 8 is supported by wooden bars (10 mm× 30 mm× ≈200 mm) for suppressing the stator vibrations. Impulses are applied to the stator and the rotor center.

Figure 9 shows impulse responses of free-run tests, showing (a) natural rotational decay characteristic, (b) displacement of upper flywheel rotor and (c) displacement of lower flywheel rotor. As shown in Figure 9(a), the

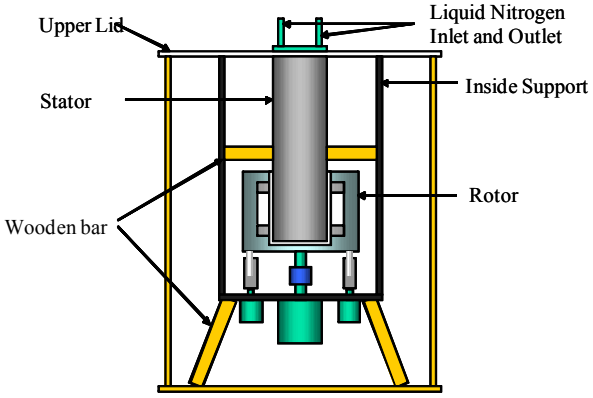


Figure 8 Experimental setup of flywheel energy storage system for impulse responses, where the stator is supported by wooden bars.

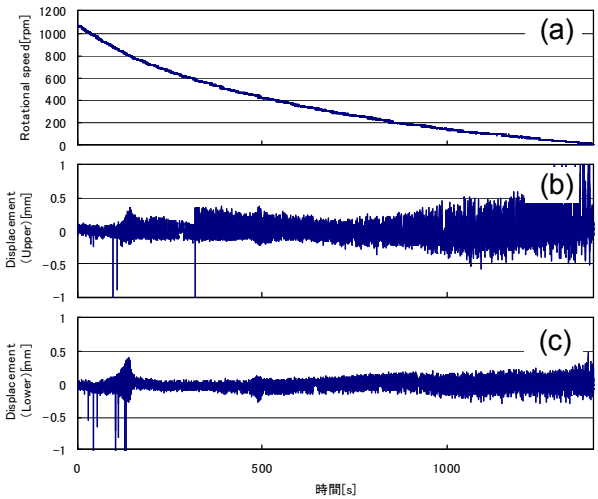


Figure 9 Experimental results of free-run test, showing (a) natural rotation decay characteristic, (b) displacement of upper flywheel rotor and (c) displacement of lower flywheel rotor

rotation speed decays from ≈1,000 rpm to zero for ≈1,200 s. There is no large displacement peak over a wide time range. However, two small peaks at rotation speeds of ≈400 rpm and ≈800 rpm are observed. These are almost equal to the rotation speeds in Figure 6.

## 4.2 Impulse responses

Figure 10 shows an experimental setup for impulse responses. The rotor is supported by four positioning actuators. The gap between rotor and stator is ≈0.8 mm. After field-cooling of superconductors in the stator, the positioning actuators separate from the flywheel rotor. The displacements of stator and rotor center are measured by using two laser displacement sensors and a FFT analyzer.

Figure 11 shows experimental results of impulse responses, showing (a) displacement of flywheel rotor and (b) its power spectrum in the case of impulses applied to the stator. As shown in Figure 11(a), the displacement

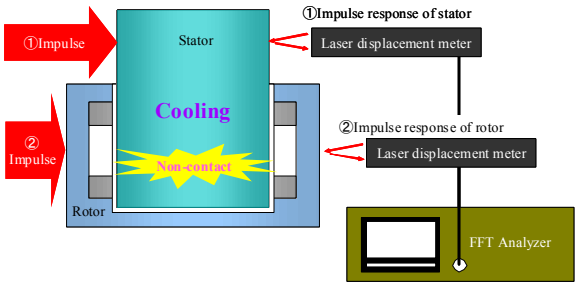


Figure 10 Experimental setup for impulse responses

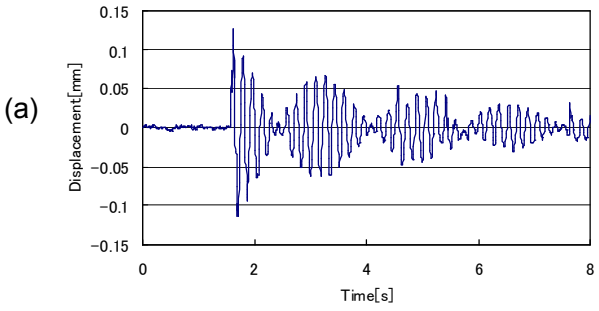


(a) Displacement characteristics

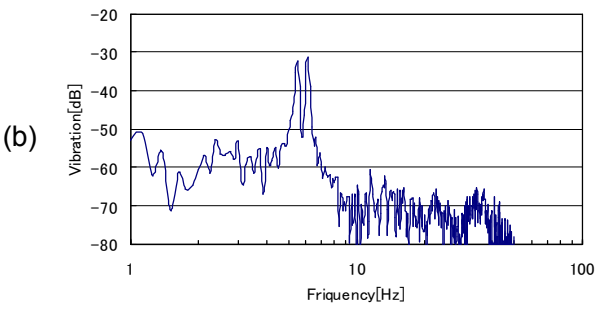


(b) Spectrum

Figure 11 Experimental results of impulse responses, showing (a) displacement of flywheel rotor and (b) its power spectrum in the case of impulses applied to the stator.

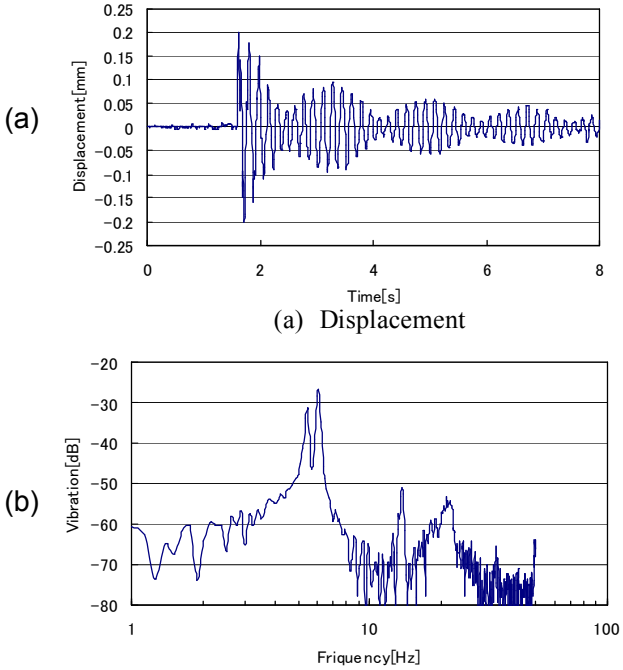


Figure 12 Experimental results of impulse responses, showing (a) displacement of flywheel rotor and (b) its power spectrum in the case of impulses applied to the rotor center

amplitude decays to ≈10% of the initial value within ≈8.0 s. However, the decay doesn't occur monotonously. This is because there are two dominant vibration modes and these modes are combined with each other. Figure 11(b) shows the peaks at 5-6 Hz and ≈12 Hz, which are corresponding to 300~360 rpm and ≈720 rpm, respectively. The frequency of 5-6 Hz in Figure 11(b) corresponds to the high frequency of Figure 11(a). However, the lower frequency of ≈3 Hz in Figure 11(a) isn't obvious in Figure 11(b).

Figure 12 shows experimental results of impulse responses, showing (a) displacement of flywheel rotor and (b) its power spectrum in the case of impulses applied to the rotor center. As shown in Figure 12(a), the displacement amplitude decays to ≈10% of the initial value within ≈8.0 s. However, the decay doesn't occur monotonously. This is because there are two dominant vibration modes and these modes are combined with each other. From Figure 12(a), two vibration modes are observed. Figure 11(b) shows the peaks at 5~6 Hz and ≈14 Hz. The peaks at 5~6 Hz and ≈13 Hz correspond to the vibration at 300~360 rpm and ≈780 rpm, respectively, as shown in Figures 6, 7 and 9.

Figure 13 shows experimental results of impulse responses, showing (a) displacement of flywheel rotor and (b) its power spectrum in the case of impulses applied to the rotor center. As shown in Figure 13(a), the displacement amplitude decays to 10 % of the initial value within ≈8.0 s. Moreover, the decay occurs monotonously. This is because there is a dominant vibration mode. From Figure 13(a), a vibration mode of ≈7 Hz is observed, which is found in Figure 13(b). The peaks at ≈9 Hz and ≈13 Hz are observed in Figure 11(b). However, the same frequencies aren't found in figure 11(a).

## 4.3 Free-run tests using eccentric load

Figure 14 shows the flywheel rotor with an aluminum load for giving an eccentricity to the flywheel rotor. The eccentric load measures ≈50 mm× ≈10 mm× ≈100 mm in size and ≈100 g in weight. Using this load, free-run

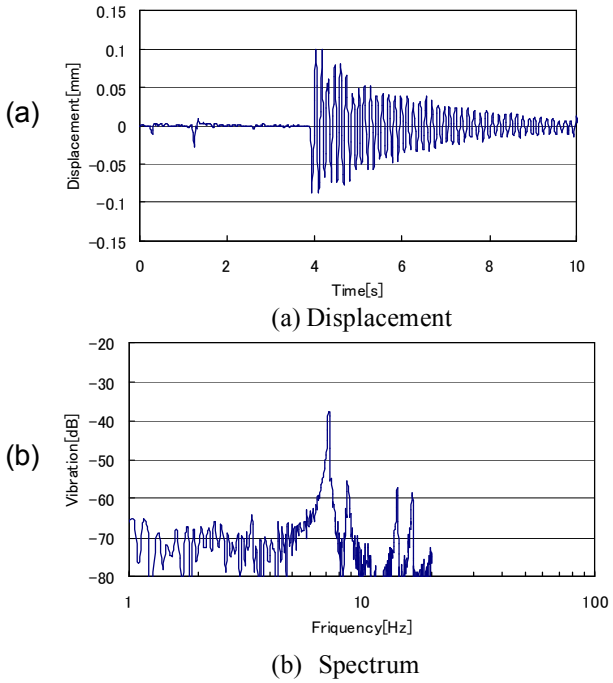


Figure 13 Experimental results of impulse responses, showing (a) displacement of flywheel rotor and (b) its power spectrum in the case of impulse responses applied to the flywheel rotor.

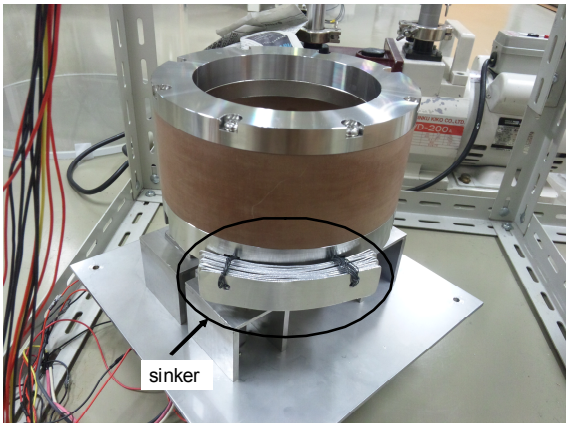


Figure 14 Flywheel rotor with an eccentric load for giving an eccentricity to the flywheel rotor

tests are performed. The rotor is supported by four positioning actuators. After field-cooling of the superconductors in the stator, the positioning actuators separate from the flywheel rotor. Just after the rotation speed increases up to 600 rpm, the driving force of the induction motor stops. These experimental procedures are the same as those of Figure 5. In this experiment, the rotor speed increases to 600 rpm because the free-run test from 1,000 rpm is regarded as dangerous. Displacements of upper flywheel rotor and lower flywheel rotor are measured by using two laser displacement sensors.

Figure 15 shows the experimental results of free-run tests, showing (a) natural rotation decay characteristic, (b) displacement of upper flywheel rotor and (c) displacement of lower flywheel rotor. From Figures 15(b) and (c), the large displacement at $\approx$400 rpm is observed. Since the superconducting stator is supported by wooden bars for suppressing the stator vibrations, the resonance rotation speed at $\approx$400 rpm is caused by the stiffness of the SMBs. The maximum displacement is $\approx$1.5 mm. Then the rotation speed decreases at time of $\approx$100 s as shown in Figure 15(a). In the time range more than $\approx$400 s, the displacement is rather larger than that in the time range less than $\approx$400 s as shown in Figures 15(b) and (c). This is because the load attached to the rotor makes the eccentric displacement larger.

Figure 16 shows the displacements of (a) upper flywheel rotor and (b) lower flywheel rotor. The result shows that the displacement pattern in Figure 16(a) is the same as that in Figure 16(b). The displacement amplitude in Figure 16(a) is more than $\approx$0.7 mm, which is upper mechanical limit of the SMBs.

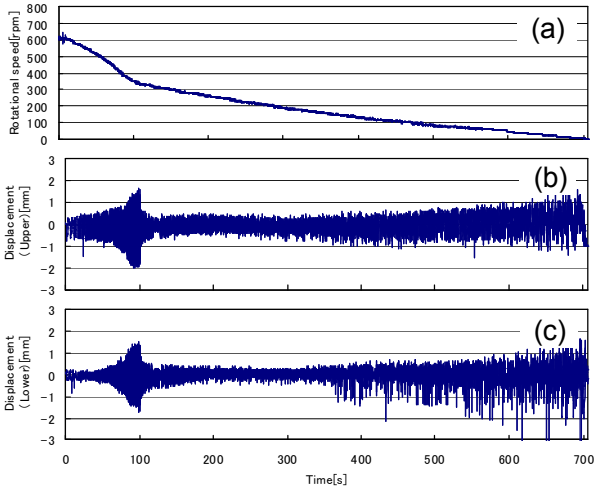


Figure 15 Experimental results of free-run tests, showing (a) natural rotation decay characteristic, (b) displacement of upper flywheel rotor and (c) displacement of lower flywheel rotor.

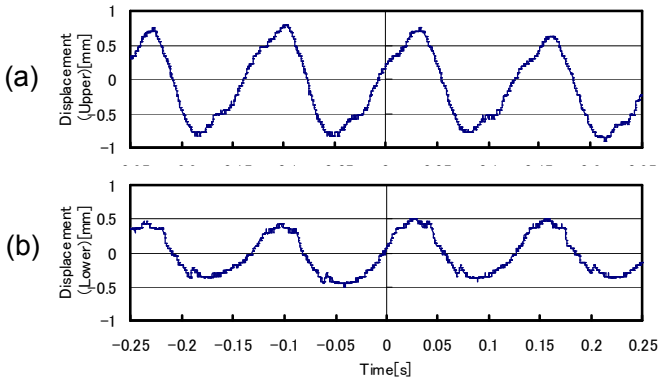


Figure 16 Displacements of (a) upper flywheel rotor and (b) lower flywheel rotor.

# 5 Summary

A new model of energy storage flywheel system is proposed. The energy storage flywheel system is composed of the superconducting stator, the flywheel rotor and the induction motor. The flywheel rotor is suspended by the stator which is fixed to the stable base. From the experimental results, the flywheel rotor spins up to 1,000 rpm by using the induction motor.

From the experiments for the flywheel system, one or two resonance rotation speeds are observed. These are caused by the stiffness of the stator or the SMBs. From the experiments for the flywheel system with an eccentric load, the large displacement at $\approx$400 rpm is observed. Since the superconducting stator is supported by wooden bars for suppressing the stator vibrations, it is found that the resonance rotation speed at $\approx$400 rpm is caused by the stiffness of the SMBs.

# References


[1] Moon, F. C. , Chang, P. -Z., *Applied Physics Letters*, 56, 397, 1990.

[2] Hull, J. R., Mulcahy, T. M., Uherka, K. L., Abboud, R. G., *IEEE Trans. Applied Superconductivity*, 5, 626, 1995.

[3] Komori, M., Tsuruta, A., Fukata, S. and Matsushita, T., *IEEE Transactions on Applied Superconductivity,* 5, 634, 1995.

[4] Okano, M., Fuchino, S., Agatsuma, K., Tamada, N., Ishii, I., Onishi, T., *J. of the Japan Society of Mechanical Engineers* (C) 62, 186, 1996.

[5] Ichihara, T., Matsunaga, K., Kita, M., Hirabayashi, I., Isono, M., Hirose, M., Yoshii, K., Kurihara, K., Saito, O., Saito, S., Murakami, M., Takabayashi, H., Natsumeda M., and Koshizuka, N., *IEEE Trans. Applied Superconductivity*, 15, 2245, 2005.